P2.9 SNOWFLAKE DISTRIBUTION CHARACTERISTICS FROM HVSD MEASURMENTS

Wanda Szyrmer*, EunSil Jung and Isztar Zawadzki
Department of Atmospheric and Oceanic Sciences, McGill University, Montreal, Quebec, Canada

1. ABSTRACT

In this study we use a large dataset of snow measurements collected by a ground-based optical disdrometer Hydrometeor Velocity and Shape Detector (HVSD). Measurements were taken at the Centre for Atmospheric Research Experiments (CARE) during winter 2005/2006 as part of the Canadian CloudSat/CALIPSO Validation Project (C3VP). The HVSD measurements provide particle size and its terminal fall speed for each interval from which the velocity- and area ratio-size relationships can be derived. Using the derived relationships and the proposed relations in the literature between the Best and Reynolds numbers, an approximate average relation between the coefficient in the experimentally obtained velocity-size relationship and the coefficient in the estimated mass power law is retrieved. The validation is made by comparing the time series of the reflectivity factor calculated from the derived mass-size relationship for a snowflake for each snow event together with the size distribution measured by the HVSD, with the reflectivity obtained from the collocated POSS (Precipitation Occurrence Sensor System) measurements. Furthermore, the snowflake size distributions are investigated in the scaling normalization framework with one and two normalizing moments, in order to develop a parameterization of snowflake size distribution, particularly with regard to the higher-order moments that are important for the mass content, reflectivity and mass- and reflectivity-weighted fall speed calculations. The obtained results agree very well with the previous studies showing that the exponential form represents a good approximation to the mean observed snowflake size distributions.

* *Corresponding author address:* Wanda Szyrmer, McGill Missouri, Dept. Atm. Ocean. Sci., Montreal, H3A2K6; e-mail: wanda.szyrmer@mcgill.ca

2. INTRODUCTION

The retrieval of microphysics of precipitating snow from Doppler radar and other remote sensing measurements, as well as snow microphysical parameterization requires knowledge of the form of the size distribution that allows an accurate derivation of the distribution moments that are important for microphysical description; moreover, the characteristics of individual snowflakes such as representative dimensional relations of mass and fallspeed are needed.

In the first part of this study we retrieved an approximate relation between the mass and terminal velocity of a single snowflake assuming that other factors, like for example the shape of the individual crystals, introduce only small correction to the average mass-velocity relationship. Subsequently, we assume here that the variability in fallspeed for snowflakes with the same size is due mainly to the particle density, and the details of the crystal types composing the aggregates have much smaller influence on the velocity.

Theoretical and laboratory work on the determination of the terminal velocity through a relation that involves the particle mass has been directed mainly to the use of the relationship between the Reynolds number, Re, determined by the product of the velocity and the size and the Best (or Davies) number, X, related to the drag coefficient and calculated from the ratio of the particle mass to the effective cross-sectional area projected on the flow. For a given type of falling particle a certain dependence of the effective area on the particle size and density is expected. For example an empirical average expression relating particle size, density and effective area has been proposed by Heymsfield et al. (2004).

The same theoretical approach based on the relation X-Re is used here to estimate the mass relations from the optical spectrograph measurements of terminal velocity and area ratio as a function of snowflake size, for different snow events. The particle mass estimation via this approach has been proposed by Hanesch (1999), Schefold (2004) or Lee et al. (2008). The next step is the determination of the approximate average relation between the coefficient in the experimentally obtained velocity-size relationships and the coefficient in the estimated mass expression.

Two types of uncertainties contribute to the uncertainty of the derived relation. The first type represent fluctuations in the measured data such as the velocity or the area ratio for a given size category, used as an important starting point for the calculations. The second type of uncertainties arises from the fact that the theoretical formulae used for the derivation of the resulting relation are not well known. These two types of uncertainties are combined when investigating the uncertainties of the derived relations.

The measurements that we use are measurements from an optical disdrometer, that can give information not only on velocity and area for each size bin of snowflake but also on snowflake particle size distribution (PSD). The measured PSDs have been used to the validation of the retrieved relation through the comparison of the expected and measured radar reflectivity time series; moreover, in the second part of this study, we investigate the measured PSDs in order to propose a snowflake PSD parameterization simple and compact, representing the measured higher order moments well. The used scaling normalization approach leads to power-law relationships between the PSD moments and does not rely on a particular functional form imposed on the PSD. However, to determine the coefficients in the relating moment power-laws, requires, in general, the knowledge of the underlying generic/intrinsic function providing an acceptable accuracy of the quantities of interest such as radar reflectivity and snow mass content, despite a very large variability of the actual PSD; therefore, these quantities of interest, as well as the available observations have to be taken into account to determine the choice of the functional form of the generic PSD function and the number and also order of normalizing moments.

Over the past years, the concept of scaling normalization has been found very convenient to describe the rain DSD (e.g. Sempere-Torres et al. 1994, Lee et al. 2004, Szyrmer et al. 2005) and for ice/snow PSD (Sekhon and Srivastava 1970, Delanoë et al. 2005, Field et al. 2005, 2007). The investigation of a general analytical form describing observed snow/ice PSD is a topic of some recent studies (Brandes et al. 2007, Heymsfield et al. 2008, Wood et al. 2008, Newman et al. 2009).

3. EXPERIMENTAL DATA USED IN THE STUDY

In this study we use a large dataset of snow measurements collected by a ground-based optical disdrometer Hydrometeor Velocity and Shape Detector (HVSD) (Barthazy et al. 2004). Measurements were taken at the Centre for Atmospheric Research Experiments (CARE) during the winter 2005/2006 as part of the Canadian CloudSat/CALIPSO Validation Project (C3VP) (Hudak et al. 2006). The HVSD measurements provide particle size and its terminal fall speed for each size class. The study of Zawadzki et al. (2009, henceforth Z09) give a detailed description of the measurements and investigate the variability in the velocity-size power-law [$u(D)=a_u D^{b_u}$] coefficient. They showed that both the depth of the precipitation system H and surface temperature T_s stratify fall velocity and the following relationship was derived by Z09:

$$a_u = 0.73 + 0.009H + 0.011T_s$$

a_u in m s^{-1} mm^{-bu}, H in km, T_s in °C.

In this study, 9 snowfall events have been selected as in Z09 by inspecting the VertiX (vertically pointing X-band radar) records and retaining only the snow systems uniform in time. An additional requirement for this study was the availability of the complete time series of the measured by HVSD spectra. For each snow event and each size bin, the mean values of velocity and area ratio, and their standard deviations were obtained from Z09 (see Table 1 for the summary of the analyzed events). Values of the measured velocity and area ratio that deviate by more than 2 standard deviations from the value expected for given size class by the obtained relations were discarded as outliers.

The data collected by the HVSD, and then the observed snowflake dimensions, correspond to the two-dimensional side view pattern. As a reference dimension *D* is chosen the maximum side-view size i.e. the maximum of the two perpendicular extensions: height of the image (vertical dimension as the snowflake falls) and width of the image (Z09). This definition of the snowflake reference size is used in our dimensional relationships obtained from measurements of the velocity and area ratio and retrieved for mass, as well in the PSDs representation.

The validation of the retrieved mass-velocity relation is made by comparing the time series of the reflectivity factor calculated for a derived mass-size relationship for an individual snowflake and applied for the size distribution measured by the HVSD, with to reflectivity obtained from the 0^{th} moment of spectrum measured by the collocated Precipitation Occurrence Sensor System (POSS). The POSS is a small X-band bistatic Doppler radar. The HVSD and POSS data are averaged over 6 minutes periods. The total number of analyzed spectra is 805.

The temperature at the ground during these events varied between -17 and -2°C. The observed reflectivity factor varied between about -10 and 35 dBZ.

4. ESTIMATION OF AVERAGE RELATIONSHIP BETWEEN SNOWFLAKE MASS AND VELOCITY OF AVERAGE RELATIONSHIP BETWEEN SNOWFLAKE MASS AND VELOCITY

4.1 Theoretical basis and main assumptions

The form of a mass-size and terminal velocity-size relationships adopted here is the most common power-law:

$$u=a_u D^{bu} \quad (1a)$$

$$m=a_m D^{bm} \quad (1b)$$

or equivalently for (1b), density-dimension relationship

$$\rho = (6/\pi) a_m D^{b_m-3} \quad (1c)$$

where *D* represents reference size of snowflake. Moreover, application of the hydrodynamic theory requires calculation of the effective area A_{eff} that is directly related to the area ratio, A_r. The area ratio is defined as

$$A_r \equiv A_{eff}/(0.25\pi D^2) = (D_{eq}/D) \quad (2)$$

As shown in Z09, two forms have been proposed for the parameterization of A_r for the side-view particle images, depending on the snowfall event:

$$A_r = a_r \left[\exp(-b_r D) - 1\right] \quad (3a)$$

$$A_r = a_{re} D^{b_{re}} \quad (3b)$$

The calculation of best estimation of mass for D-size snowflake from its fallspeed is based on the determined relation between the Reynolds number Re and the Best (or Davies) number X related to the drag coefficient but having no dependence on fallspeed. The two numbers are defined as (e.g. List and Schemenauer 1970):

$$\mathrm{Re} = \frac{u D_*}{\nu} \quad (4)$$

$$X = C_D \cdot \mathrm{Re}^2 = \frac{2g}{\rho_a \nu^2} \frac{m D_*^2}{A_{eff\perp}} \quad (5)$$

taking $\rho_{snow} - \rho_{air} \approx \rho_{snow}$. The environmental conditions are included via the kinematic viscosity and air density ν and ρ_a, respectively. *g* denotes gravitational acceleration. The expression for ***X*** contains the mass *m* and the effective particle area projected normal to the flow $A_{eff\perp}$ in addition to D_* that denotes the chosen characteristic dimension of the particle. Introducing the area ratio normal to the flow, $A_{r\perp}$ and using (2) ***X*** can be expressed as

$$X = \frac{8g}{\pi \rho_a \nu^2} \frac{m}{A_{r\perp}} \left(\frac{D_*}{D_\perp} \right)^2 \quad (6)$$

$D_\perp$ is the maximum diameter in the direction normal to the flow that (what does that refer to?) is not measurable and therefore must be estimated. The final expression for **X** depends on the choice of the characteristic size D_*. Taking D_* equal to the maximum diameter projected on the flow and assuming an idealized spheroidal shape for the snowflakes $D_\perp$, Böhm (1992) modified (6) by introducing the fourth root of the inverse of area ratio and the axial ratio ϕ of this assumed oblate spheroid shape of snowflake:

$$X = \frac{2g}{\rho_a \nu^2} \frac{m}{(A_{r\perp})^{1/4} \max[\phi, 1]} \quad (7)$$

A theoretical relationship between Re and X derived from the boundary layer theory was developed by Böhm (1989) and Mitchell (1996) on the basis of the previous work of Abraham (1970) in the form :

$$\mathrm{Re}=\frac{\delta_0{}^2}{4}\left[\left(1+\frac{4X^{1/2}}{\delta_0{}^2C_0{}^{1/2}}\right)^{1/2}-1\right]^2 \qquad (8)$$

with the two constants δ_0 and C_0 characterizing the boundary layer shape and thickness. For aggregates, Mitchell and Heymsfield (2005) modified slightly the relation by adding an empirical term $-a_0X^{b_0}$. Khvorostyanov and Curry (2005) proposed an alternate method to introduce this correction. In this study, the particle mass is deduced from the Best number that is calculated from Re. Therefore, we need to invert the proposed relations Re=f(X). Equation (8) can be directly inverted while the two other relations Re=f(X) were inverted by fitting log(X) to a 6th order polynomial of log(Re):

$$\log(X)=\sum_{l=1}^{6}C_l\left[\log(\mathrm{Re})\right]^l \qquad (9)$$

with the constants C_l.

Snowflake size and area measured by the HVSD represent a side-view of the particle. In general, the falling snowflakes, due to aerodynamic forcing, are oriented preferably horizontally. On average, their horizontal dimension is larger than the value measured when viewed on side-projection (e.g. Magono and Nakamura 1965; Matrosov et al. 2005; results from the Snowflake Video Imager, SVI, deployed in Canada for C3PV during winter 2006/07). Since the horizontal, flow-normal dimensions that are required for the velocity calculations cannot be measured, they must be estimated from the side projection.

The relations used to estimate the horizontal projection dimensions are based on 1) the assumption that $A_{r\perp}\approx A_r$ i.e. the area ratio is independent of the angle of observation, normal or parallel to the flow, and 2) the relation from Schefold (2004) giving the ratio of the effective area projected normally to the flow to the area from the side view, given as a function of the canting angle α and the side projected axial ratio ε. The latter is the quotient of the side projected minor axis to the side projected major axis:
$$f_A\equiv\frac{A_{eff\perp}}{A_{eff}}\approx\varepsilon_{\min}+(1-\varepsilon)\cdot\left[\frac{1}{\varepsilon_{\min}}\left(\frac{\alpha}{90^0}-1\right)+1\right] \qquad (10)$$
where $\varepsilon_{\min}$ describes the minimal value of the axis ratio evaluated from the measurements. The last relation together with the assumption $A_{r\perp}\approx A_r$ is also used to calculate the maximum horizontal dimension $D_\perp$ from the maximum side dimension D taken as reference dimension.

4.2. Steps in the derivation of the mass-velocity relationship

An average relation between a snowflake mass and velocity has been derived in the following steps with the four first steps calculated separately for each snow event:

i) Calculation of Re from the HVSD measurements of terminal velocity and area ratio.

ii) Estimation of the value of X from Re using (8) and the two versions of (9).

iii) Best estimation of mass for D-size snowflake from the estimated **X** and area ratio normal to the flow. For each size-bin 36 different values of mass is calculated from different combinations of the applied relations (X-Re relationships, expressions of **X**, smoothed and no smoothed measured *u* and A_r, different approaches to define the characteristic size), each value of mass is considered as the 'measured' value of mass using different method and interrelated through the common parameters, their geometric weighted mean is taken as the best estimation of the snowflake mass with reference diameter *D*. The weight of each 'measured' mass is the reciprocal of the corresponding uncertainty obtained by combining the contribution of the uncertainty related to the different quantities involved having the estimated uncertainties shown in Table 2. The uncertainty of the best estimated mass is done by calculating only the maximum uncertainty that is simply the linear sum of the weighted uncertainties of an individual mass values, otherwise, the existing correlations between the different components makes the calculations of the resulting uncertainty very complex. The results of the calculations for one snow event are shown as an example in Fig.1.

iv) Determination by regression of the coefficients in the power-law relation *m-D* given by (1b) from the best estimated mass for each *D*. An example is shown Fig. 1 where the blue line shows the best-fit power law. For the studied 9 snow events, the obtained coefficients a_m and b_m and their values are quoted in Table 1 and shown in Fig. 2. For comparison, the mean value obtained by Brandes et al. (2007) from a very large dataset is also superposed in Fig. 2. However, because *D* in their study was taken as equivalent diameter, their relation has been recalculated using the average relation D_{eq} -*D* obtained from our data: $D_{eq} = 0.688 D^{0.95}$ (in CGS units). The results of Bringi et al. (2008) for individual snow events, shown also in Fig.2, have been recalculated as for Brandes's result.

v) From all events, derivation by regression an average relation between the power-law coefficients in the mass and velocity dimensional relationships. This relation is obtained for the mass and velocity exponents fixed at 2 and 0.18, respectively. The value of 2 corresponds to effective snowflake density decreasing with size as D^{-1} [$\rho = (6/\pi) m D^{-3} = (6/\pi) a_m D^{-3+b_m}$] and is in good agreement with numerous observational studies of snow at the surface (Mitchell et al. 1990 from the overall observed particle types; Brandes et al. 2007) and aircraft observations (e.g. Heymsfield et al. 2002) as well with theoretical studies (Westbrook et al. 2004). The derived values of b_m in the present study, shown in Fig. 2 for analyzed snow events, cluster between the value of 1.8 and 2.1. Taking into account all these factors together with the general uncertainty in the mass-size relation, we set the exponent b_m to 2 for power law relation representing the precipitating snow; the coefficient a_m becomes then the only coefficient to be determined in the mass-size relationship. On the other hand, the obtained by Z09 velocity power laws of the form (1a) for different homogenous snow events, show the relatively small variability of the exponent b_u. Since we are looking for simplified relations, the value of b_u is fixed at 0.18. The best values of a_u for b_u=0.18 were obtained via least squares method from the data for each event. In Fig. 3 the values of a_m derived for b_m=2 and b_u=0.18 are plotted as a function of the velocity coefficient a_u obtained from the data. Each point represents one of the 9 events. The analytical relation between a_m and a_u is assumed to have the form:

$$\log a_m = \alpha + \beta a_u \qquad (12)$$

Coefficients α and β have been determined by least squares regression with the weighting factor equal to $1/[\Delta(\log a_m)]^2$ for each [a_u, log(a_m)] pair. The uncertainty of the coefficient a_u is not taken into account, its value has been included in the uncertainty of retrieved a_m. The solid line in Fig. 3 represents the least squares fitting squares with $\alpha = -2.92$ and $\beta = 0.00558$ in the CGS units.

4.3. Validation

In this study the snowflake mass/density retrieval process use the measured reflectivity, to validate the retrieved mass-size relationships. For each snowfall event, the mass coefficient is estimated from the velocity coefficient $\boldsymbol{a_u}$ using (12). Knowing the mass-size relationship, the backscatter cross section of each size category is calculated from Model 5 described in Fabry and Szyrmer (1999). The expected reflectivity factor is then computed from the snowflake size distributions measured by the HVSD. The time series of the calculated reflectivity are compared with the reflectivity derived from the collocated POSS. The HVSD and POSS data are averaged over 6 minutes periods. The scatter plot of reflectivity calculated for the all 9 events versus the POSS measured reflectivity is presented in Fig. 4. The root mean standard error (RMSE), is equal to 2.86 dB. Fig. 5 presents an example of the reflectivity time series. The black line gives the POSS measured reflectivity, while the blue line is the reflectivity calculated from the mass relationship derived for the given event. The red line show the reflectivity calculated for the same spectra but using the mass relation retrieved for the event of 2006-Jan 09.

4.4. Application

With (12) and the information about the PSD, the reflectivity- and mass-weighted velocity or snow precipitation rate can be calculated together with the reflectivity factor. In Fig. 6 the reflectivity-weighted velocity U_Z is plotted against the reflectivity as obtained from the calculations for all snow events. The solid lines are obtained through regression for assumed following linear relation between U_z and Ze in dBZ and log($\boldsymbol{a_m}$):

$$U_Z = 365 + 0.484 Z_e[dBZ] + 120\log(a_m) \qquad (13)$$

U_Z and a_m are in the CGS units.

In Fig. 7, the calculated snow precipitation rate S is plotted as a function of the calculated Ze. Four empirical relations reported in the previous studies are also shown in this figure.

5. PARAMETERIZATION OF SNOWFLAKE PSDs MEASURED BY HVSD WITHIN SCALING NORMALIZATION FRAMEWORK

Measured variables related to the PSD are:

- PSD function: *n(D)*, where *n(D)dD* is a concentration of particles between *D* and *D+dD*; measured is n_D: particle concentration in size bin D; the scattergram of all 805 measured 6-min averaged spectra composed of 16574 counts is shown in Fig. 8;
- PSD bulk/integral representation by the PSD moments of different orders *p*:

$$M_p \equiv \int D^p\, n(D)\, dD$$

from measurements:

$$M_p \approx \sum_{D_{\min}}^{D_{\max}} D^p n_D$$

The use of the power-law form to describe the dimensional relations for various specific properties of individual particles, such as mass and fall-speed, leads to the bulk quantities of PSD expressed in terms of the PSD moments.

The PSD normalization is based on the assumption that the distributions are self-similar and depend only on the normalizing PSD moments. This approach naturally gives rise to the occurrence of power law relationships between different PSD moments with the scaling/normalizing moments relating all other moments to each other. For a given self-preserving distribution, the actual PSD can be calculated from the normalizing moments. Characteristic sizes such as mean-volume diameter are defined in terms of two moments as: $D_{i,j} \equiv \left(\mathrm{M}_j/\mathrm{M}_i\right)^{1/(j-i)}$. For the snowflake density assumed to change with (1/*D*), i.e. for a_m in (1b) equal to 2, the mean mass-weighted diameter is given by $D_{2,3} = \mathrm{M}_3 / \mathrm{M}_2$.

In an one-moment scheme 1-M with the *i*th moment M_i of the distribution used as the normalizing moment the normalized PSD function is given by $g(x_i) = n(D, \mathrm{M}_i)\mathrm{M}_i^{-\alpha_i}$, with $x_i \equiv D\mathrm{M}_i^{-\beta_i}$ and $\alpha_i + (i+1)\beta_i = 1$. The resulting expression relating any *p*th moment to the normalizing moment is:

$$\mathrm{M}_p = C_p^{(i)}\, \mathrm{M}_i^{1+(p-i)\beta_i} \tag{14}$$

where the coefficient $C_p^{(i)}$, is the moment of order *p* of $g(x_i)$:

$$C_p^{(i)} \equiv \int_0^\infty x_i^{\,p}\, g(x_i)\, dx_i\,.$$

In the two-moment (2-M) normalization, the general form of the normalized PSD is written as:

$$h(x_{i,j}) = n(D, \mathrm{M}_i, \mathrm{M}_j)\, \mathrm{M}_i^{-(j+1)/(j-i)}\, \mathrm{M}_j^{(i+1)/(j-i)},$$

where M_i and M_j are two normalizing moments and $x_{i,j} \equiv D\left(\mathrm{M}_i/\mathrm{M}_j\right)^{1/(j-i)}$. It follows that any moment of order *p* can be obtained from:

$$\mathrm{M}_p = C_p^{(i,j)}\, \mathrm{M}_i^{(j-p)/(j-i)}\, \mathrm{M}_j^{(p-i)/(j-i)} \tag{15}$$

with $C_p^{(i,j)} = \int_0^\infty x_{i,j}^p\, h(x_{i,j})\, dx$. The generic function given by $g(x_i)$ or $h(x_{i,j})$ is independent of the value of normalizing moments and is called the generic (intrinsic) distribution function. Its form remains free, but in order to determine the coefficients C_p it has to be fixed. The accuracy of the estimated moments M_p is limited by this inherent assumption of a fixed shape for the distribution.

We investigate our dataset of the snowflake PSDs with the second and third moments as normalizing moments, as in Field et al. (2005, 2007). These two moments are assumed to be not affected by the truncation effect during the measurements. The tested schemes are: 1-M(2), 1-M(3) and 2-M(2,3), where the two former are one-moment schemes and the latter two-moment scheme. The normalization with the 3 schemes of our dataset from Fig. 8 is shown in Fig. 9. In the 1-M schemes, the values the scaling exponents, β_2 and β_3, are 0.208 and 0.252, respectively. They are derived following the procedure from Sempere-Torres et al. (1998) using weighted total least squares fitting. The comparison of the scatter of data points in Fig. 9 with Fig. 8 shows that the use of normalization overcomes to some extent the issues of the variability of the shape of the PSD. Consequently, the dependence of the relations between the moments (the coefficients C_p) on the variability of the PSD shape is reduced, particularly in the 2-M normalization.

In Fig. 9 the average functions obtained from the data points are shown as solid color lines (except red) with bars indicating standard deviation. The over plotted red lines represent an exponential function in the following forms:

1-M schemes:

$$g(x_i) = \left[\Gamma(1+i)\right]^{-1} \lambda_i^{\,i+1} \exp\left[-\lambda_i\, x_i\right]$$

with $\lambda_2 = 4.01$ and $\lambda_3 = 6.78$;

2-M scheme:

$$h(x_{2,3}) = 13.5\exp[-3x_{2,3}].$$

These forms satisfy the self-consistency constraints: $C_i^{(i)} = 1$ for 1-M and $C_i^{(i,j)} = C_j^{(i,j)} = 1$ for 2-M. In general, the exponential distribution is very close to the average generic function, except at the smallest sizes. The derived coefficients in the moment-relating power-law (14) for the two 1-M schemes are plotted in Fig. 10 as a function of the order of the derived moment. Also, in the same figure, the exponents, calculated from the derived values of β_i, are shown.

The exponential function is a special case of the Generalized Gamma (GG) function that is very flexible in shape having two shape parameters μ and α:

$$f_{GG}(x) = A_0(\lambda x)^{\mu}\exp\left[-(\lambda x)^{\alpha}\right],$$

A_0 is a normalization factor, and λ is a scaling parameter. 5 forms of $f_{GG}(x)$ corresponding to different combinations of the two shape parameters are plotted in Fig. 11. Because of its flexibility, the function GG has been chosen to the further investigation of the best representation of the observed PSDs of snowflakes using the 2-M(2,3) scheme.

To evaluate the uncertainties in the retrieved moments using 2-M(2,3) scheme combined with the GG function, we use the Standard Deviation of Fractional Error (SDFE), defined as:

$$SDFE \equiv \left[\frac{1}{n}\sum\left(\frac{M_{p,mes}-M_{p,est}}{M_{p,mes}}\right)^2\right]^{1/2} \quad (16)$$

where n is the total number of spectra, $M_{p,mes}$ and $M_{p,est}$ are the pth moment from measurement and from estimation, respectively. Fig. 12 displays a contour map of log(SDFE) in the space of the two f_{GG} shape parameters. The presented results are for the moments M_1 and M_4. The point representing exponential form is shown by a red "x" symbol. From this contour plots, it can be seen that the minimum SDFE area is a broad valley with very small changes in SDFE that spans over the whole presented range of the two shape parameters. With the constraint α=1 that corresponds to the modified gamma function, the results presented in Fig. 12 show that the value of μ=0, i.e. exponential form, is a good choice with respect to the retrieved moments M_1 and M_4.

Limiting our investigation to the generic normalized PSD in the exponential form, SDFE in the moment estimate is calculated using the 3 schemes. The results are plotted in Fig. 13 as a function of the order of the estimated moment. The average value of the ratio F_M defined for the moment of order p as $M_{p,mes}/M_{p,est}$ is also plotted in the same figure. A quantitative comparison of the accuracy of the 3 schemes can be done from the results presented in Fig. 13. In the 1-M(2) scheme, SDFE increase very rapidly for high moments because of relatively important scatter of $g(x_2)$ at larger normalized sizes as shown in Fig. 9. A very good accuracy is obtained with the 2-M(2,3) scheme, SDFE is less than about 0.3 at the overall range of p. For higher order moments, all 3 schemes become progressively underestimating with increasing moment order. The presented results for low order moments are affected by the truncation from the sampling, and therefore are highly biased.

Fig. 14 shows scatterplots for all dataset of the estimated 4th order moment *vs* the measured. Each graph shows the results for each scheme. For the scheme 2-M(2,3), the scatterplot lie very close along a 1:1 line. In general, for all 3 schemes the convergence becomes better for the lower values of the moment, i.e. for the PSDs with the smaller volume- (or mass-) weighted size.

6. SUMMARY

To reduce the number of parameters describing an individual snowflake with size D, we propose an approximate relation between its mass and velocity, assuming that other factors, like for example the shape of the individual crystals, introduce negligible correction to the average mass-velocity relationship. The power law exponents describing derived mass-size relation and obtained directly from measurement velocity-size relation have been set to the fixed values of 2 and 0.18, respectively.

The validation of the results is made by comparing the time series of the reflectivity factor calculated for a derived mass-size relationship for an individual snowflake and applied for the size distribution measured by the HVSD, with to reflectivity obtained from the 0th moment of spectrum measured by the collocated POSS. Moreover the obtained mass-velocity relation together with the PSDs measured by HVSD is also used to derive an approximate average expression relating the reflectivity-weighted velocity to the radar reflectivity and mass/density of falling snow.

The measured snowflake PSDs have been investigated in the scaling normalization framework using the schemes 1-M(2), 1-M(3) and 2-M(2,3) in order to determine an analytical function that well represent the higher-order moments of the snowflake PSDs and to compare the accuracy of the moment estimation using different schemes. It is concluded as in the previous investigations of the ice/snow PSDs (e.g. Brandes et al. 2007, Heymsfield et al. 2008) that the exponential distribution assure relatively accurate estimates the higher-order moments. In general, the one moment scheme 1-M(3) appear to be much more accurate than 1-M(2) for the higher moment estimation. The moment scheme 2-M(2,3) provide very accurate estimation of the observed higher-order moments.

The parameterization proposed by Field et al. (2005 and 2007) for the schemes 1-M(2) and 2-M(2,3) has been applied to our dataset. In general, their parameterization with the two-moment scheme, using the sum of exponential and gamma functions, produce a very accurate estimates of the observed moments. However, their moment-relating power laws with the temperature dependence and the 2nd order normalizing moment give an important SDFE for higher order moments. Probably it is related to the fact that the temperature of snow in this study is relatively high (>-17°C) compared to the large interval of temperature corresponding to their studies.

7. REFFERENCES

Abraham, F.F., 1970: Functional dependence of drag coefficient of a sphere on Reynolds number. *Phys. Fluids*, 13, 2194-2195.

Barthazy, E., S. Göke, R. Schefold and D. Högl, 2004: An optical array instrument for shape and fall velocity measurements of hydrometeors. *J. Atmos. Ocean. Technol.,* 21, 1400–1416.

Böhm H., 1989: A general equation for the terminal fall speed of solid hydrometeors. *J. Atmos. Sci.*, 46, 2419–2427.

Böhm, 1992: A general hydrodynamic theory for mixed-phase microphysics. Part I: drag and fall speed of hydrometeors. *J. Atmos. Res.*, 27, 253–274.

Brandes, E. A., K. Ikeda, G. Zhang, M. Schönhuber, and R. Rasmussen, 2007: A Statistical and physical description of hydrometeor distributions in Colorado snow storms using a video disdrometer. *J. Appl. Meteor. Climatol.*, 46, 634-650.

Brandes, E.A., K. Ikeda, G. Thompson, M. Schönhuber, 2008 : Aggregate terminal velocity/temperature relations. *J. Appl. Meteor. Climatol*, 47, 2729-2736.

Bringi, V.N., GJ Huang, D. Hudak, R. Cifelli, S.A. Rutledge, 2008: A methodology to derive radar reflectivity-liquid equivalent snow rate relations using C-band radar and a 2D video disdrometer. ERAD 2008 – The Fifth European Conference on Radar in meteorology and Hydrology.

Delanoë, J., A. Protat, J. Testud, D. Bouniol, A. J. Heymsfield, A. Bansemer, P. R. A. Brown and R.M. Forbes, 2005: Statistical properties of the normalized ice particle size distribution. *J.Geophys. Res.*, 110, D10201, doi:10.1029/2004JD005405

Fabry, F., and W. Szyrmer, 1999: Modeling of the melting layer. Part II: Electromagnetics, *J. Atmos. Sci.*, 56, 3593-3600.

Field, P. R., R. J. Hogan, P. R. A. Brown, A. J. Illingworth, T. W., Choularton, and R. J. Cotton, 2005: Parameterization of iceparticle size distributions for mid-latitude stratiform cloud. *Quart. J. Roy. Meteor. Soc.,* 131, 1997–2017.

Field P. R., A. J. Heymsfield, and A. Bansemer, 2007: Snow size distribution parameterization for midlatitude and tropical ice clouds. *J. Atmos. Sci.*, 64, 4346–4365.

Fujiyoshi, Y. T. Endoh, T. Yamada, K. Tsuboki, Y. Tachibana, and G. Wakahama, 1990: Determination of a ***Z-R*** Relationship for snowfall using a radar and high sensitivity snow gauges. *J. Appl. Meteor.,* **29,** 147–152.

Hanesch, M., 1999: Fall velocity and shape of snowflakes. Ph.D. thesis. Diss. ETH No. 13322. 111 pp.

Heymsfield, A.J., A. Bansemer, L.S. Durden,J.E. Dye,. W. Hall, and C.A. Grainger, 2002: Observations and parameterizations of particle size distributions in deep tropical cirrus and stratiform precipitating clouds: Results from in situ TRMM field campaigns. *J. Atmos. Sci.*, **59**, 3457-3491.

Heymsfield, A.J., A. Bansemer, C. Schmitt, C. Twohy, and M. R. Poellot, 2004: Effective ice particle densities derived from aircraft data. *J. Atmos. Sci.*, 61, 982-1003.

Heymsfield, A.J., P.Field, A.Bansemer, 2008: Exponential size distributions for snow. *J. Atmos. Sci.*, 65, 4017–4031.

Hudak, D., H. Barker, P. Rodriguez, and D. Donovan, 2006a: The Canadian CloudSat Validation Project. 4th European Conf. on Radar in Hydrology and Meteorology, Barcelona, Spain, 18-22 Sept., 2006, 609-612.

Khvorostyanov, V. I., and J. A. Curry, 2005: Fall velocities of hydrometeors in the atmosphere: refinements to a continuous power law. *J. Atmos. Sci.*,62, 4343-4357.

Lee, G.W., A. Heymsfield, I. Zawadzki, D. Hudak, E. Jung, P. Rodriguez, F. Fabry, A. Bansemer, B. Sheppard, 2008: Snow microphysical processes and variation of effective density - diameter relationships. ERAD 2008, 7.2.

Lee, G. W., I. Zawadzki, W. Szyrmer, D. Sempere-Torres, and R. Uijlenhoet, 2004: A general approach to double-moment normalization of drop size distributions. *J. Appl. Meteor.*, 43, 264–281.

List, R., R.S. Schemenauer, 1970: Free-fall behavior of planar snow crystals, conical graupel and small hail. *J. Atmos. Sci.,* 28, 110-115.

Magono, C, and T. Nakamura, 1965: Aerodynamic studies of falling snowflakes. *J. Meteor. Soc. Japan*, 43, 139-147.

Matrosov, S.Y., R. F. Reinking, and I. V. Djalalova, 2005: Inferring fall attitudes of pristine dendritic crystals from polarimetric radar data. *J. Atmos. Sci.,* 62, 241–250

Mitchell D. L., 1996: Use of mass- and area-dimensional power laws for determining precipitation particle terminal velocities. *J. Atmos. Sci.*, 53, 1710–1723.

Mitchell, D. L., and A. J. Heymsfield, 2005: Refinements in the treatment of ice particle terminal velocities, highlighting aggregates., *J. Atmos. Sci.,* 62: 1637-1644.

Mitchell, D. L., R. Zang, and R. L. Pitter, 1990: Mass-dimensional relationships for ice particles and the influence of riming on snowfall rates. *J. Appl. Meteor*., 9, 903-910.

Newman, A.J., P.A. Kucera, C.R. Williams, L.F. Bliven, 2009: Snowflake size spectra retrieved from a UHF vertical profiler. *J. Atmos. Oceanic Technol*., 26, 180-199.

Ohtake, T., and T. Henmi, 1970: Radar reflectivity of aggregated snowflakes. Preprints, 14th Radar Meteorology Conf., Tucson, AMS, 209-210.

Schefold, R.: Messungen von Schneeflocken: Die Fallgeschwindigkeit und eine Absch¨atzung weiterer Grössen, ETH-Diss. Nr. 15431, 2004.

Sekhon, R. S., and R. C. Srivastava, 1970: Snow size spectra and radar reflectivity. *J. Atmos. Sci.,* 27, 299–307.

Sempere-Torres, D., J. M. Porrà, and J. D. Creutin, 1994: A general formulation for raindrop size distribution. *J. Appl. Meteor.,* 33, 1494–1502.

Szyrmer, W., S.Laroche and I.Zawadzki. 2005: A microphysical bulk formulation based on scaling normalization of the particle size distribution. Part I: Description. *J. Atmos. Sci.*, 62, 4206–4221.

Westbrook, C. D., R. C. Ball, P. R. Field, and A. J. Heymsfield, 2004: Universality in snowflake aggregation. *Geophys. Res. Lett.,* 31, L15104, doi:10.1029/2004GL020363.

Woods, C.P., M.T. Stoelinga, J.D. Locatelli, 2008: Size spectra of snow particles measured in wintertime precipitation in the Pacific Northwest. *J. Atmos. Sci*: 65, 189–205.

Zawadzki, I., E. Jung, G.W. Lee, 2009: , Snow studies. Part I: A study of natural variability of snow terminal velocity. submitted to *J. Atmos. Sci*.

Zawadzki, I., P. Zwack and A. Frigon, 1993: A study of a CASP storm: Analysis of radar data. *Atmos.-Ocean*, 31, 175-199.

TABLES

Symbol	Events	a_u	b_u	a_m	b_m	a_m for b_m=2	a_m for b_m=2 from (12)
◇	2005 Nov 24 20:00-21:20	120.1	0.15	4.52e-3	1.80	5.58e-3	5.76e-3
□	2006 Jan 06 20:30-22:20	82.0	0.22	3.53e-3	2.10	3.39e-3	3.42e-3
◇	2006 Jan 09 08:00-08:25	147.9	0.17	8.20e-3	1.94	8.58e-3	8.21e-3
◇	2006 Feb 06 17:30-18:30	96.6	0.14	4.25e-3	1.88	4.56e-3	4.30e-3
△	2006 Feb 11 00:00-03:00	94.3	0.13	4.06e-3	1.90	4.39e-3	4.21e-3
△	2006 Feb 18 17:10-18:10	110.0	0.19	3.99e-3	1.79	5.21e-3	5.28e-3
△	2006 Feb 28 00:10-01:00	99.8	0.20	3.37e-3	1.83	4.11e-3	3.99e-3
△	2006 Feb 28 04:30-06:30	99.2	0.18	2.93e-3	1.80	3.90e-3	4.23e-3
□	2006 Feb 28 10:30-12:30	91.1	0.14	3.35e-3	1.80	3.87e-3	3.89e-3

Table 1. Summary of the characteristics of the analyzed events. All parameters are given in the CGS units. The symbol color from red to dark violet corresponds to temperature of measurement from -2*°C* to -17*°C*. The events associated with a deep system (>3 *km*) are described by a diamond, with moderate system (1.5 *km* to 3 *km*) by a triangle, while a square is used to represent shallow systems.

X-Re relation	f_A	ϕ	u	A_r
30 %	30 %	30 %	20 %	20 %

Table 2. Assumed range of uncertainty for the variables used to estimate ***m-D*** relationship

FIGURES

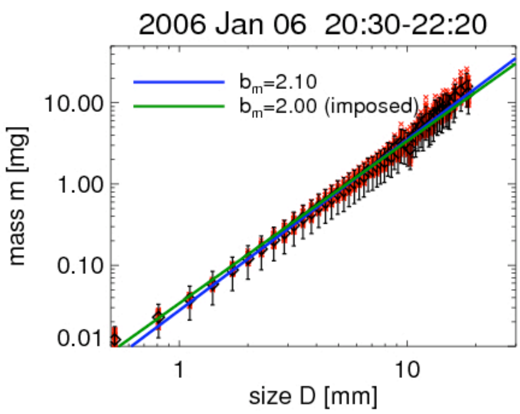

Fig.1 Example of calculated the mass-size relationship for one snowfall event. The size *D* on the *x*-axis represents the snowflake side-view maximal extension. The red plus signs correspond to the values obtained from different combinations of the used relations. The black diamonds represent the geometric mean taken as the best estimate of snowflake mass of size *D*. Their estimated uncertainty is shown by the error bars. Solid blue and green lines represent the least squares regression with the value of b_m from fitting and fixed at 2, respectively.

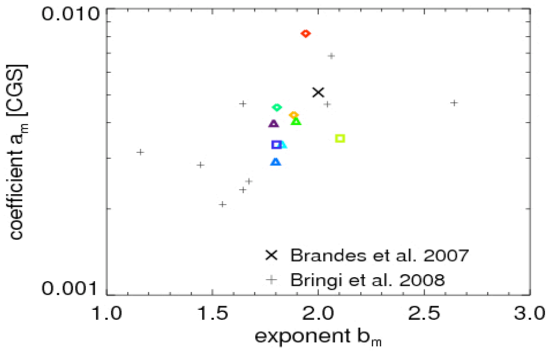

Fig.2 Estimated parameters in the mass-size power law for the 9 analyzed snow events. For comparison, the set of the mean relation parameters obtained by Brandes *et al.* (2007) is also plotted, together with the results of Bringi *et al.* (2008) for individual snow events. Our average relation between D and D_{eq} was used to recalculate the parameters since their relations are in terms of D_{eq}.

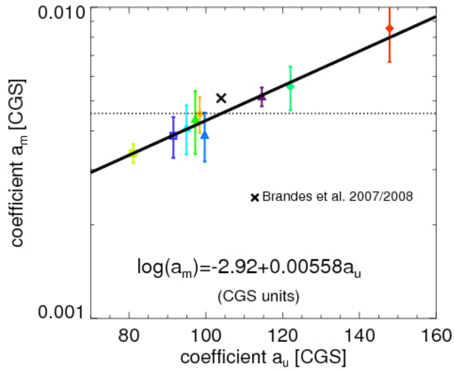

Fig.3 Mean relationship between the coefficients in the mass and velocity power laws with fixed exponents of b_m=2 and b_u=0.18. Solid line shows the linear best-fit. The dotted line gives the average value of a_m for all events.

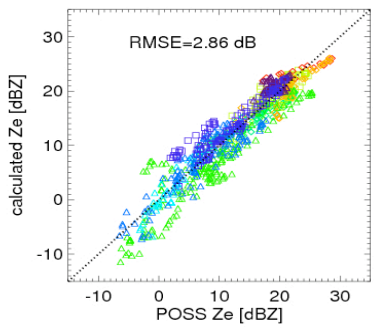

Fig.4 Scatterplot for all events of the calculated Z_e from the estimated mass relationship for each event and the time series of size spectra measured by HVSD versus the Z_e measured by POSS. The RMSE (Root Mean Standard Error) is equal to 2.86 *dB*.

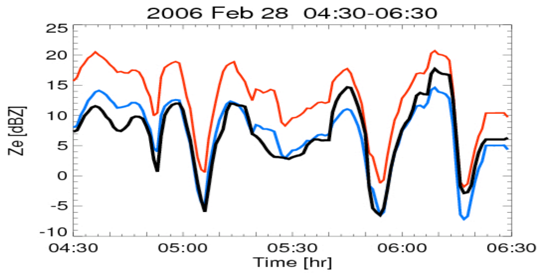

Fig.5 Example of time series plot of Z_e. The black line shows the POSS measured Z_e; the blue line gives the calculated Z_e from the HVSD spectra with mass power coefficient a_m derived from the velocity coefficient a_u for the presented event, while the red line shows the calculation results for a_m retrieved for the event of 2006-Jan-09. The POSS measured Z_e and HVSD spectra are averaged over a 6 minute period.

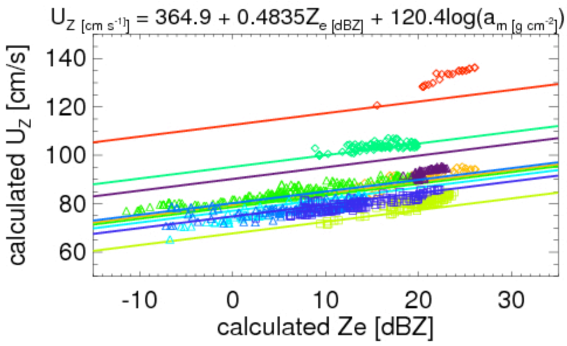

Fig.6 Calculated reflectivity-weighted velocity U_Z vs calculated reflectivity Z_e for all data points. The solid lines show the approximate linear relation obtained through regression between U_Z and Z_e and the mass coefficient a_m.

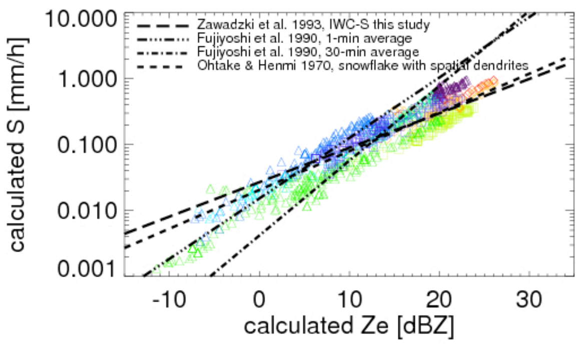

Fig.7 Relation between snow precipitation rate S and reflectivity factor Z_e calculated for the estimated mass relationship. For comparison, the black lines show four empirical relations from different studies.

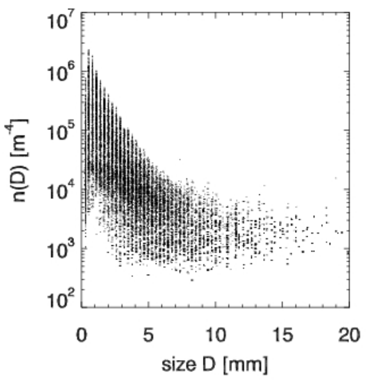

Fig.8 Scattergram of 805 analyzed snowflake PSDs with 16574 counts. Time period for averaging is 6 minutes.

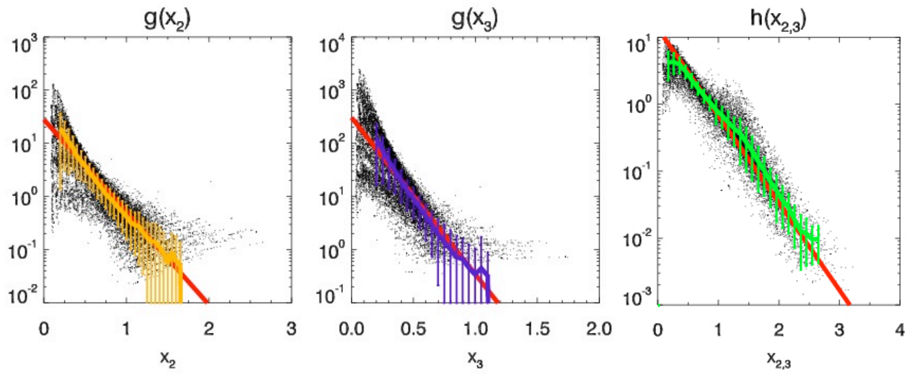

Fig.9 Scattergrams of the normalized PSDs with 3 schemes: 1-*M*(2), 1-*M*(3), 2-*M*(2,3). The red lines show the exponential form, while the other color line show the average normalized distribution with bars indicating standard deviation.

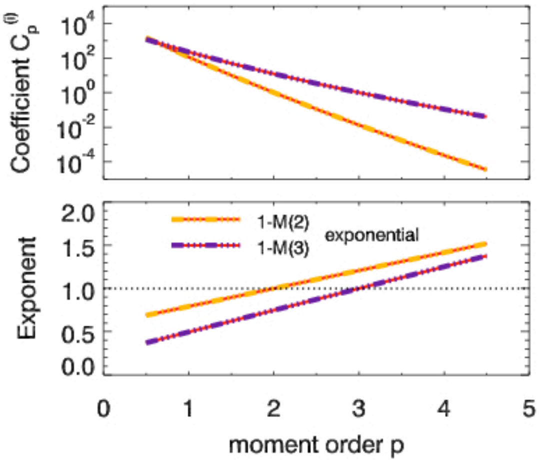

Fig.10 Coefficient $C_p^{(i)}$ and exponent in the moment-relating power-law in the two investigated 1-*M* schemes as a function of the moment order. The exponential form is used to calculate the value of $C_p^{(i)}$.

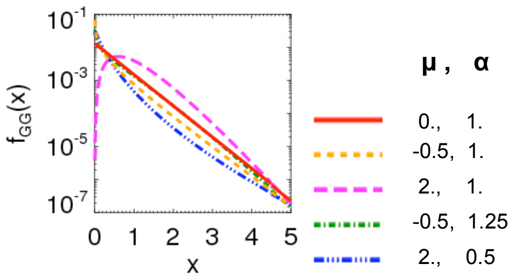

Fig.11 Five forms of the generalized gamma (GG) function.

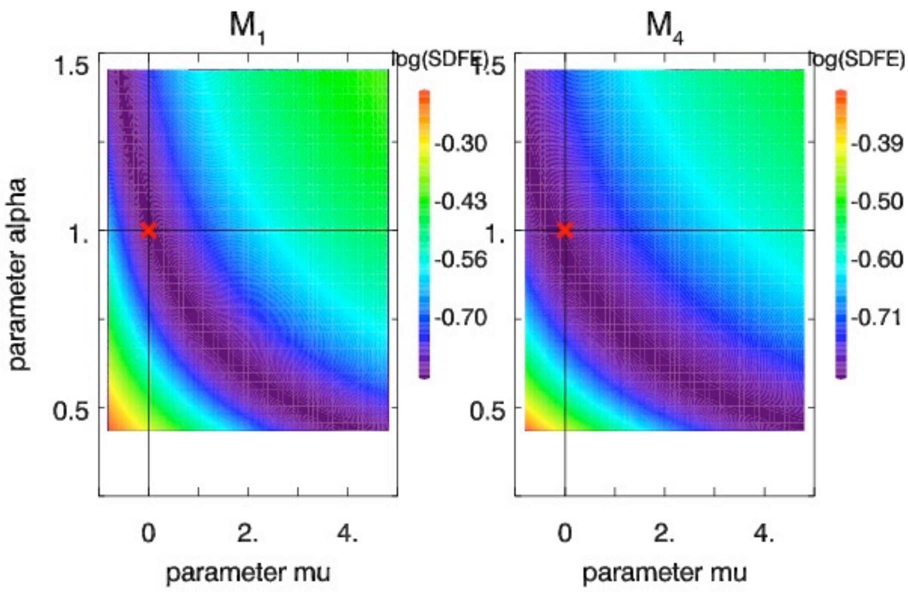

Fig.10. Contour of *log(SDFE)* (SDFE: Standard Deviation of Fractional Error) for the moments M_1 and M_4 in the two shape parameters space for the generalized gamma analytical function in the two-moment normalization 2-M(2,3).

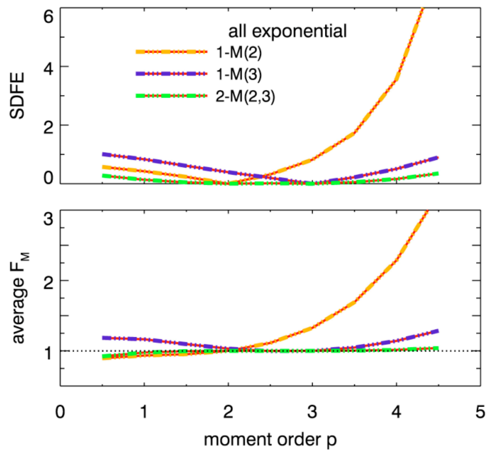

Fig.11. SDFE and average ratio of observed to estimated moments as a function of the moment order calculated for the 3 schemes.

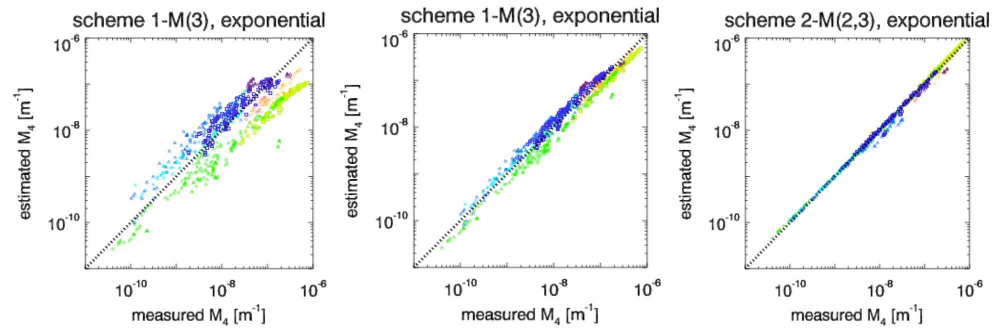

Fig.12 Scatterplots of the measured 4th order moment vs the estimated by the 3 schemes.